

## STANDING WAVE EFFECTS IN MICROWAVE ELLIP-SOMETRY

**L. R. Lawson**

Bradford, PA 16701, USA

**H. A. Yousif**

Physical and Computational Sciences Division  
University of Pittsburgh at Bradford  
Bradford, PA 16701, USA

**Abstract**—Unlike ellipsometry using light, ellipsometry using microwaves can be subject to significant standing wave effects resulting from reflection of the received wave back to the source. This paper examines these effects on the apparent homogeneity of circular polarization. These effects are examined experimentally using an ellipsometer with no sample and compared with calculated results for a single order of reflection. Good agreement is obtained. That the peak-to-peak variations in the observed irradiance are on the order of four times the amplitude reflectance is observed. The angular dependencies of these effects are path length dependent.

### 1. INTRODUCTION

The authors have found microwave ellipsometry useful for studying the fiber structure of wood and wood composites. While the literature on microwave ellipsometry is not extensive, microwave ellipsometry has been used for measuring the properties of metals, semiconductors, the earth's surface thick coatings and building materials [1–4]. In the process of studying wood composites, the authors noticed systematic deviations in the measured angular distribution of scattered irradiance of fibers from theoretical predictions. These deviations are due to standing waves resulting from the reflection of the source irradiation by the detector back to the source and again back to the detector. The effects of these standing waves manifested themselves through

---

Corresponding author: H. A. Yousif (yousif@pitt.edu).

noticeable phase shifts that are perceivable since the size of the apparatus is in the order of ten times the wavelength. They are surprisingly strong for relatively small (lumped single-round-trip) amplitude reflection coefficients. In ellipsometry using light, standing wave effects are not seen. Therefore, the authors think that this study might provide useful information for other researchers because some have noted problems with accuracy when using this method [5].

The presence of a standing wave gives rise to three separate phenomena that are clearly observed when the specimen is removed, and source and detector are aligned. These three phenomena are:

1. The intensity at the detector varies sinusoidally with the path length from the source to the detector with a spatial period that equals half that of the source wavelength. The peak-to-peak magnitude of this variation divided by the mean signal strength is roughly four times the amplitude reflectance coefficient. Thus, in our apparatus with no specimen between the source and the detector, 8% of the signal amplitude is reflected back to the detector in the first pass, and as a result the strength of the detected signal varies by nearly one third as the detector is moved through a distance of  $\lambda/2$ , where  $\lambda$  is the vacuum wavelength of radiation used.

2. It is difficult to obtain truly circularly polarized radiation at the source. A brief description of a circular polarizer in the microwave region is given in Section 2.

If the quarter-wave plate at the source is adjusted to provide circular polarization, the apparent polarization at the detector is elliptical, and, as the polarization of the detector is rotated through an angle,  $\omega$ , the detected signal intensity traces out an ellipse. See Fig. 1 for the definition of  $\omega$  and other angles used. The rotation of this ellipse varies as the detector is moved to change the total path length. It is consistent with the sinusoidal variation just described.

3. When the source is adjusted for circular polarization and the analyzer quarter-wave plate is rotated through an angle,  $\psi$  (See the caption of Fig. 1), the extinction curve departs from the expected cosine-squared relation, the Law of Malus, by an amount that depends on the separation between the source and the detector. When the analyzer quarter wave plate is aligned relative to that at the source to give a half wave retardance ( $\psi = 0$ ), no signal is observed at the detector as would be expected. In the presence of a specimen these phenomena are modified by the geometrical and optical properties of the specimen. Finally, we will describe the previous phenomena using Jones matrices for calculating these effects.

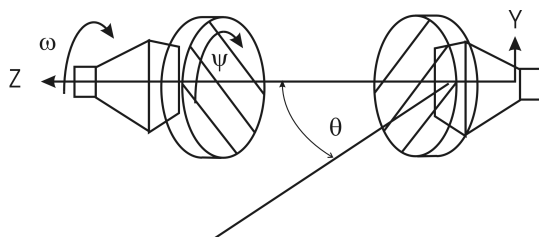


**Figure 1.** Summary of angular relations. The detector is on the left followed by the two wave plates and then the source. The  $y$ - and  $z$ -axes are indicated. The horizontal plane is the  $xz$ -plane.  $\omega$  is the angle between the detector's electric polarization and the  $x$ -axis. The electric polarization of the source is aligned with the  $x$ -axis. The fast axes of the wave plates are parallel to the lines shown across their faces. The fast axis of the source wave plate is inclined  $45^\circ$  to the  $x$ -axis, as shown, to give circular polarization. That of the detector, the "analyzer" is also aligned  $45^\circ$  to the  $x$ -axis when  $\psi = 0$  so that there is no measured signal at the detector.  $\psi$  is thus the inclination of the fast axis with respect to the  $x$ -axis minus  $45^\circ$ .  $\theta$  is the angle in the horizontal plane between the  $z$ -axis and the detector when the irradiance distribution (Fig. 5) is measured.

## 2. THE ELLIPSOMETER

The ellipsometer uses two  $9.5 \text{ cm} \times 7.5 \text{ cm}$  horns for source and detector with a path length of 1 m. The detector is a diode biased to operate as a linear square-law detector. The source used for these tests was a diode operating at a wavelength,  $\lambda$ , of 2.857 cm (manufacturer's nominal). The detector is mounted on the radial arm of a motor driven goniometer. The specimen mount is located at the center of the arm's rotation. Two quarter-wave plates are provided, one for the source and the other for the detector, which are mounted in front of the horns. Either may be removed. The quarter wave plates were fabricated using parallel metal slats supported with Styrofoam<sup>TM</sup> following a suggestion given by van Vliet and DeGraauw [6]. The slats are made of aluminum 2.812 cm wide and of sufficient length to traverse the horn in any orientation. The plates are spaced in parallel, 2.037 cm apart. Approximately 2.04 cm of the width of each slat is embedded in the Styrofoam<sup>TM</sup> dielectric. The assembly is tuned to the frequency precisely by adjusting this depth of penetration using a surface plate and digital height gage. In operation the incident wave is resolved into two perpendicular components. That component with the  $E$ -vector parallel to the length direction of the plates is guided and

has a higher phase velocity than the other component that has the  $E$ -vector perpendicular to length of the plates, which is unguided. In addition to the principal goniometer previously mentioned, an auxiliary goniometer with a center located at the source, and a radius of 1 m, was fitted for the purpose of examining the radiation pattern.

### 3. CALCULATION OF STANDING WAVE EFFECTS

The Jones matrix formalism was used to calculate the effects of standing waves. In this approach the wave being operated upon is defined by a complex 2-vector giving the  $E$ -component in the  $x$ -direction and that in the  $y$ -direction respectively (see Fig. 1).

Complex numbers are used to represent phase relations. Operators are usually Cartesian tensors and can be rotated by matrix rotation to represent physical rotation of the optical element. A sequence of optical events is represented by a sequence of matrix multiplications. In laying out this sequence one must take care to note which operators commute and which do not. Tables of operators and further discussion of the method are given in elementary texts on physical optics [7]. The Jones matrices used are defined in Table 1 below.

In the above table,  $\mathbf{Q}_{45}$  denotes a quarter wave plate with the fast axis at  $45^\circ$  to the  $x$ -axis.  $\mathbf{Q}(\pi/4 + \psi)$  denotes a quarter wave plate with the fast axis rotated an additional  $\psi$  radians with respect to that of  $\mathbf{Q}_{45}$ .  $\mathbf{SP}(kx)$  denotes a phase delay equal to the product of the distance  $x$  times the scalar value of the wave vector,  $k$ .  $\mathbf{LP}(\omega)$  denotes a linear polarizer rotated  $\omega$  radians with respect to the  $x$ -axis.

In the case of the apparent uniformity of circular polarization, the contribution of the incident wave is given by,

$$\mathbf{E}_1 = \mathbf{Q}_{45} \cdot \mathbf{E}_x. \quad (1)$$

**Table 1.** Definitions of various symbols used in Jones Matrix.

Operator	Symbol
$E$ -horizontally polarized wave (vector)	$\mathbf{E}_x$
Quarter wave plate at $45^\circ$	$\mathbf{Q}_{45}$
Reflection (identity matrix times scalar)	$\mathbf{R}$
Phase delay (identity matrix times complex exponential)	$\mathbf{SP}(kx)$
Linear polarizer	$\mathbf{LP}(\omega)$
Rotated quarter wave plate	$\mathbf{Q}(\pi/4 + \psi)$

The contribution from first order reflection is given by,

$$\mathbf{E}_2 = \mathbf{Q}_{45} \cdot \mathbf{Q}_{45} \cdot \mathbf{SP}(2\varphi) \cdot \mathbf{R} \cdot \mathbf{Q}_{45} \cdot \mathbf{E}_x, \quad (2)$$

where  $\varphi = kx$ .  $k$  is  $2\pi$  divided by the wavelength,  $\lambda$ , and  $x$  is the separation between the source and the detector. Note that Eqs. (1) and (2) have some common factors removed. The amplitude at the detector is then found as,

$$\mathbf{E} = \mathbf{LP}(\omega) \cdot (\mathbf{E}_1 + \mathbf{E}_2). \quad (3)$$

The normalized irradiance is then,

$$I = (\mathbf{E}_1 \mathbf{E}_1^* + \mathbf{E}_2 \mathbf{E}_2^*) f, \quad (4)$$

where  $*$  denotes complex conjugation.  $\mathbf{E}_1$  and  $\mathbf{E}_2$  are the two components of  $\mathbf{E}$ , and  $f$  is the chosen normalizing factor. This factor is the reciprocal of  $\sup(\mathbf{E}_1 \mathbf{E}_1^* + \mathbf{E}_2 \mathbf{E}_2^*)$ .

In the case of crossed circular polarizers, the incident wave is given by,

$$\mathbf{E}_1 = \mathbf{Q}(\pi/4 + \psi) \cdot \mathbf{Q}_{45} \cdot \mathbf{E}_x. \quad (5)$$

The contribution from the first order reflection is given by,

$$\mathbf{E}_2 = \mathbf{Q}(\pi/4 + \psi) \cdot \mathbf{Q}_{45} \cdot \mathbf{R} \cdot \mathbf{Q}_{45} \cdot \mathbf{Q}(\pi/4 + \psi) \cdot \mathbf{SP}(2\varphi) \cdot \mathbf{Q}(\pi/4 + \psi) \cdot \mathbf{Q}_{45} \cdot \mathbf{E}_x. \quad (6)$$

The irradiance is obtained using (3) and (4) with  $\omega$  set to zero.

In these cases the calculations were performed using MAPLE<sup>TM</sup>. The symbolic expressions obtained were not compact in the sense of easily being written on a page, and there seems no point in reporting them. Calculations using higher order reflections were also not performed because they would make (6) too long to report. Furthermore, graphing the results suggested simple approximations to specific cases. The reader may extend this calculation by inserting an additional Jones matrix to represent his/her particular specimen and also find approximations to suit specific cases and specimens.

#### 4. EXPERIMENTAL

By fitting experiment to the theory above, we determined that the amplitude reflection coefficient which constitutes the diagonal elements of  $\mathbf{R}$  is 0.086. This value is used in the comparisons which follow. This value is an approximation. It is likely that the two diagonal elements differ because the diode detector absorbs some of the signal in its direction of polarization. However, complicating the model seems useless since it would not alter the quality of the effects being presented but would add confusion. In the graphs which illustrate the

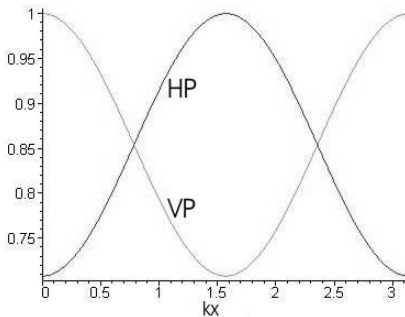
examples to follow, data points will be plotted when they differ from the calculated curves but not otherwise.

Figure 2 plots the horizontally and vertically polarized irradiances vs.  $kx$  at a fixed angle  $\omega = 0$ , in the presence of reflection. It is immaterial which of the two curves is which since the origin is not specified. Note that the peak-to-peak amplitude is about 4 times the scalar reflection coefficient. The period of these oscillations is half the incident wavelength because irradiance (power) is proportional to the amplitude squared. The two electric polarizations, called horizontal and vertical, have a relative lag of one quarter the incident wavelength due to the circular polarization of the incident wave.

Figure 3 plots the irradiance as a function of the polarization angle,  $\omega$ , for three fixed values of  $kx$ . In the absence of reflection, these ellipses would be circles.

The case of “crossed circular polarizers” is analogous to that of crossed linear polarizers. A quarter wave plate is fixed at the circular polarizing angle, near  $45^\circ$ , at the source. A second quarter wave plate is placed at the detector and rotated. Here at the angle zero, the two plates have their fast axes aligned, and the detected irradiance is therefore zero as shown in Fig. 4, the extinction curve. The angle of greatest extinction is defined as zero. At an angle of  $\psi = \pi/2$ , a maximum in detector irradiance is reached.

The data points on the experimental extinction curve in general do not plot as the law of Malus, the sine squared in this style of plot. Rather in this example they lie close to the inner curve in Fig. 4 which is calculated for the same reflection coefficient, 0.086 as used for the



**Figure 2.** Irradiance vs. source to detector distance. HP indicates the horizontal component; VP indicates the vertical component. The origin is chosen for clarity.

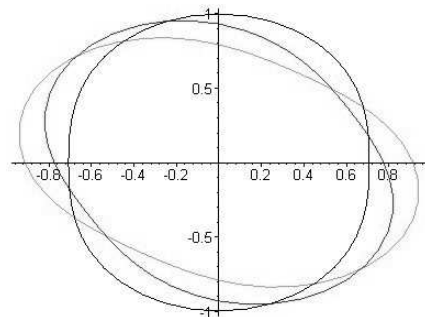


**Figure 3.** Polar plots of irradiance vs.  $\omega$  for  $kx = 0, 0.5$  and 1 radian.

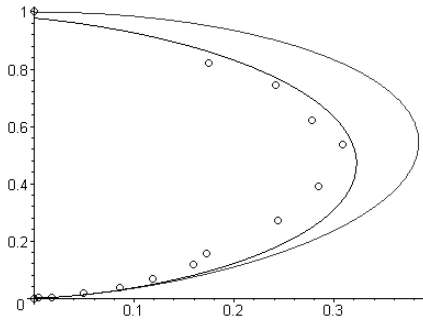


**Figure 4.** Polar plot of irradiance vs. detector wave plate angle,  $\psi$ , for crossed circular wave plates. The inner line represents the case where the reflection is phase shifted by  $-0.87$  radian. The outer line is the law of Malus. Note that the scaling of the  $x$ - and  $y$ -axes differs.

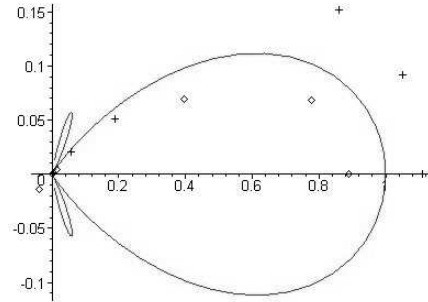


**Figure 5.** Polar plot of the source irradiance distribution in the horizontal plane where  $kx = 0.7$  radian. Diamonds indicate vertical electric polarization; crosses indicate horizontal electric polarization. The solid line is the calculated value where no reflection is present. Note that the scaling of the  $x$ - and  $y$ -axes differs.

other plots and a phase delay for the reflection of  $kx = -0.87$  radian. The outer curve represents the law of Malus which would apply in the absence of reflection.

In addition to these investigations, the effect of reflection on the irradiance distribution was also investigated. An example is plotted in Fig. 5 where irradiance for circularly polarized radiation incident radiation is measured with a linearly polarized detector. Irradiance is plotted as a function of angle,  $\theta$ , in the horizontal plane. In Fig. 5, the crosses indicate data points for the horizontally polarized component while diamonds indicate data points for the vertically polarized component. The solid line indicates the calculated irradiance distribution of the horn. Note the inequality between the two polarizations. This results from the phenomenon described in Fig. 3.

The error in these measurements from all sources is estimated to be not greater than  $\pm 11\%$  for all graphs shown except for Fig. 5 where the maximum error is estimated as closer to  $15\%$ . The noise floor, the rms fluctuation in the dc offset, is  $3.2\text{ mV}$  or  $0.06\%$  of full signal.

## 5. CONCLUSION

The high reflectivity of horn transducers and the long wavelength of microwaves compared with light give rise to standing wave effects not seen in light ellipsometry. These effects can distort ellipsometric measurements unless they are specifically taken into consideration through calculated corrections or the use of a non-reflecting detector. On the other hand, they need not be entirely a nuisance. They could be the basis for an interferometric method for measuring changes in optical path length as might occur due to non-uniformities in a dielectric material.

## ACKNOWLEDGMENT

The authors acknowledge the assistance provided by Bradford Forest Products Inc.

## REFERENCES

1. Sakurai, T., S. Mochizuki, and M. Ishigame, "Measurement of electrical conductivity of oxides at high temperatures by microwave ellipsometry," *High-temp.-High Press.*, Vol. 7, 411–417, 1975.
2. Hertl, S., G. Schaffar, and H. Storl, "Contactless determination of the properties of water films on roads," *J. Phys. E (Sci. Instrum.)*, Vol. 21, 955–958, 1988.
3. Sagnard, F., F. Bentabet, and C. Vignat, "Theoretical study of method based on ellipsometry for measurement of complex permittivity of materials," *Electronics Letters*, Vol. 36, 1843–1845, 2000.
4. Tsuzkiyama, K., T. Sakai, T. Yamazaki, and O. Hashimoto, "Ellipsometry for measurement of complex dielectric permittivity in millimeter-wave region" *Conf. Proc. 33rd European Microwave Conference*, 487–490, 2003.
5. Mochizuki, S. and T. Sakurai, "Electrical conduction of MgO doped with CR at high temperatures in oxidizing atmosphere," *Phys. Stat. Sol.*, Vol. 41, 411–415, 1977.
6. Van Vliet, A. H. F. and T. de Graauw, "Quarter wave plates for submillimeter wavelengths," *Int. J. Infrared and Millimeter Waves*, Vol. 2, 465–476, 1981.
7. Hecht, E. and A. Zajac, *Optics*, Addison-Wesley, Reading Mass., 1974.